Dynamic response model of the human leg
by Douglas Wayne Johnson

A thesis submitted in partial fulfillment of the requirements for the degree of MASTER OF SCIENCE in Mechanical Engineering
Montana State University

Abstract:
A three-dimensional finite element dynamic response model of the lower human leg was constructed for the purpose of simulating the vibrational response of a leg subject to harmonic excitation. The model consists of the major structural components of the leg (tibia, fibula, flesh, and interosseous ligament), and includes viscoelastic and support condition parameters. Several methods were used to reduce the system array size and speed up computation time. The results are presented in the form of eight test response runs, each of which was done altering material property parameters. Comparisons between experimental and analytical data indicated that flesh damping, end condition stiffness, and interosseous ligament stiffness all played a major role in determining leg vibrational response.

STATEMENT OF PERMISSION TO COPY

In presenting this thesis in partial fulfillment of the requirements for an advanced degree at Montana State University, I agree that the Library shall make it freely available for inspection. I further agree that permission for extensive copying of this thesis for scholarly purposes may be granted by my major professor, or in his absence, by the Director of Libraries. It is understood that any copying or publication of this thesis for financial gain shall not be allowed without my written permission.

Signature Douglas W. Johnson

Date 10/19/78

DYNAMIC RESPONSE MODEL OF THE HUMAN LEG

by

DOUGLAS WAYNE JOHNSON

A thesis submitted in partial fulfillment
of the requirements for the degree

of

MASTER OF SCIENCE

in

Mechanical Engineering

Approved:

Dennis O. Blackketter
Chairperson, Graduate Committee

Dennis O. Blackketter
Head, Major Department

Henry L Parsons
Graduate Dean

MONTANA STATE UNIVERSITY
Bozeman, Montana

October, 1978

ACKNOWLEDGEMENT

The author wishes to thank Dr. Dennis Blackketter for his continuing support throughout the year. The author would also like to thank Dr. Edward Garner for his wisdom and knowledge on the subject of bone shaking.

TABLE OF CONTENTS

	Page
VITA	ii
ACKNOWLEDGEMENT	iii
LIST OF TABLES	v
LIST OF FIGURES	vi
ABSTRACT	vii
CHAPTER I: REVIEW	1
CHAPTER II: THE MODEL	4
CHAPTER III: RESULTS	15
CHAPTER IV: CONCLUSION	34
APPENDIX I: MASS AND STIFFNESS ARRAYS	36
APPENDIX II: COMPUTER PROGRAM	41
REFERENCES	44

LIST OF TABLES

	Page
TABLE 1.--Bone Properties	16
TABLE 2.--Flesh Properties	16
TABLE 3.--Interosseous Ligament Properties	17
TABLE 4.--Summary of Runs	20

LIST OF FIGURES

	Page
FIGURE 1.--Typical Leg Cross Section	5
FIGURE 2.--Rheological Model	8
FIGURE 3.--Typical Beam Element	9
FIGURE 4.--Lower Leg Bone Structure	11
FIGURE 5.--Transducer Locations (Right Leg)	19
FIGURE 6.--Response Plot (Run 1)	21
FIGURE 7.--Response Plot (Run 2)	22
FIGURE 8.--Response Plot (Experimental)	23
FIGURE 9.--Mode Diagram (Run 1)	25
FIGURE 10.--Response Plot (Run 3)	26
FIGURE 11.--Response Plot (Run 4)	27
FIGURE 12.--Response Plot (Run 5)	29
FIGURE 13.--Response Plot (Run 6)	30
FIGURE 14.--Mode Diagram (Run 6)	31
FIGURE 15.--Response Plot (Run 7)	32
FIGURE 16.--Response Plot (Run 8)	33
FIGURE I-1.--Mass ($\underset{\sim}{M}$) and Stiffness ($\underset{\sim}{K}$) Arrays	39
FIGURE II-1.--Flow Diagram	42

ABSTRACT

A three-dimensional finite element dynamic response model of the lower human leg was constructed for the purpose of simulating the vibrational response of a leg subject to harmonic excitation. The model consists of the major structural components of the leg (tibia, fibula, flesh, and interosseous ligament), and includes viscoelastic and support condition parameters. Several methods were used to reduce the system array size and speed up computation time. The results are presented in the form of eight test response runs, each of which was done altering material property parameters. Comparisons between experimental and analytical data indicated that flesh damping, end condition stiffness, and interosseous ligament stiffness all played a major role in determining leg vibrational response.

CHAPTER I

REVIEW

In recent years methods involving 'in vivo' materials testing of long bones have gained increased interest. One particular technique involves the development of response plots of frequency vs. amplitude for a bone as it is excited in the range of its first bending resonance frequency by low amplitude sinusoidal input. The shape of these plots are a function of the stiffness, geometry, and damping in the system. 'In vivo' tissue mechanical properties can be derived by accurately modeling the system and adjusting parameters until the response predicted by the model matches experimental data. Several models have been proposed for the purpose of predicting 'in-vivo' long bone response due to harmonic excitation.

Jurist [1] modeled the human ulna with three relatively simple models and compared predicted results with experimental results of previous tests. The ulna was modeled as an elastic homogeneous cylindrical beam with different end conditions comprising the three models. Jurist assumed that his response plots were measuring the resonance caused by the first bending mode of vibration, and correlated bone stiffness, geometry, and mineral content with respect to this first natural frequency.

Doherty [2] indicates that rigid body motion might be the dominant mode in the first resonance peak observed by Jurist, and concludes that these tests might be more a test of bone mass and end condition stiff-

ness than of bone stiffness. Jurist [3], however, using a fourth rigid body model demonstrated a low correlation between rigid body motion and experimental results.

Orne [4] added viscoelastic properties to Jurist's pinned end beam model and attempted to match his analytical results with experimental impedance test data. Because of abnormally high bone damping necessary to match results, Orne concludes that considerable damping is produced by the surrounding flesh, and that further models should include flesh. In a later model, Orne [5] added a lumped mass flesh system to his model and was able to more accurately mathc experimental results.

Garner and Blackketter [6] constructed a finite element model of the entire forearm including both the ulna and radius along with surrounding flesh. Matching theoretical and experimental response plots, Garner was able to obtain both flesh and bone viscoelastic material properties. However, since only one arm was modeled and tested, no statistical verification of his results could be established.

Although a number of models have been proposed, the validity of 'in vivo' dynamic response measurements as a means of predicting biological tissue properties has not been established.

It is the intent of this research to construct a finite element dynamic response model of the human lower leg for the purpose of material property evaluation. This model will incorporate techniques utilized by Garner, with various modifications. The model will include

viscoelastic bone and flesh properties as well as variable end conditions to allow rigid body motion. The proposed model will also be capable of quickly matching geometric properties with those of a given x-ray in an attempt to handle large population samples.

The following sections describe the modeling techniques in more detail as well as the effects of different viscoelastic parameters on vibrational response. Finally, general comments are made about modeling and experimental techniques involving long bone vibrational testing, with recommendations for both.

CHAPTER II

THE MODEL

The human leg is a complicated biological system consisting of two bones, tibia and fibula, connected to various types of soft tissue. For this reason, the finite element method was chosen as best suited to accurately model the lower leg. Also, because of the high degree of damping apparent from experimental response plots, the model includes viscoelastic properties.

The model can be visualized as a series of ten leg segments obtained by slicing the lower leg at eleven equally spaced cross sections from the knee to the ankle. Each segment contains two beam elements, representing the tibia and fibula, and fifteen hexahedron flesh elements surrounding the bones. Figure 1 is a typical computer generated cross section showing the bone and flesh elements as well as the flesh tie in points. These flesh tie in points are assumed to be rigidly attached to the bone.

The resulting finite element matrix equation in the Laplace domain is

$$[(s^2 \underset{\sim}{M} + \underset{\sim}{K}_b(s) + \underset{\sim}{K}_f(s)]\ \underline{U}(s) = \underline{F}(s) \qquad (1)$$

where $\underset{\sim}{M}$, $\underset{\sim}{K}_b(s)$, and $\underset{\sim}{K}_f(s)$ are the combined bone and flesh mass array, bone stiffness array, and flesh combined stiffness array respectively. The Laplace variable is s while $\underline{U}(s)$ and $\underline{F}(s)$ are displacement and force vectors. Note that due to the viscoelastic behavior of the material,

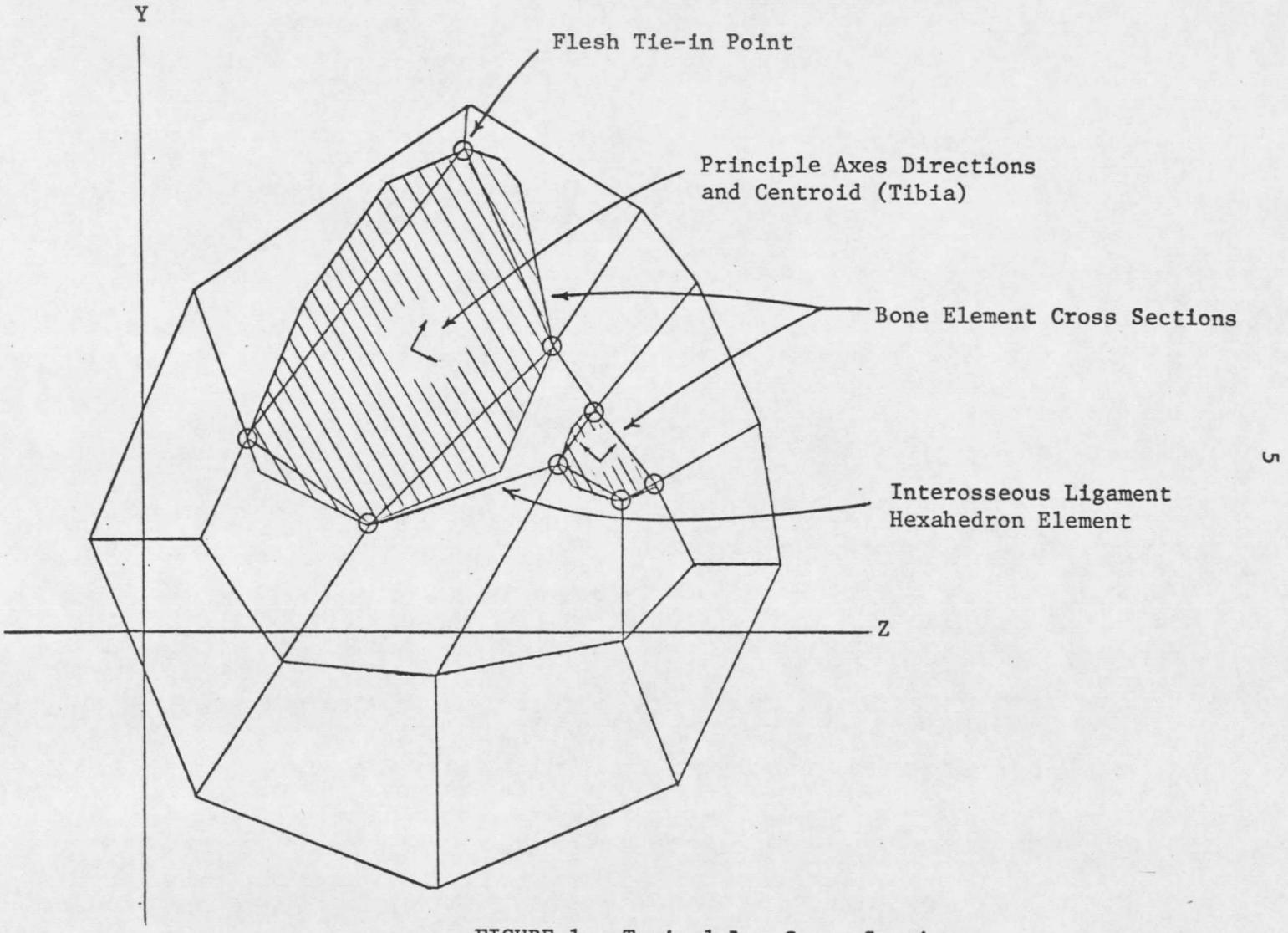

FIGURE 1.--Typical Leg Cross Section

the stiffness arrays become functions of the Laplace variable. For steady state harmonic motion, Equation 1 can be solved in the time domain by using the relationship

$$s = j\omega$$

where j is the complex indicator and ω is frequency. The result is a set of complex simultaneous equations of the form

$$\underset{\sim}{D}(j\omega)\ \underline{U}(j\omega) = \underline{F}(j\omega) \tag{2}$$

where $\underset{\sim}{D}(j\omega) = (-\omega^2 \underset{\sim}{M} + \underset{\sim}{K}_b(j\omega) + \underset{\sim}{K}_f(j\omega)]$

which can be solved for displacement amplitudes by using any complex simultaneous equation routine available on a computer.

Viscoelastic Model

The viscoelastic constituative laws for linear three dimensional viscoelastic materials in the Laplace domain may be divided into deviatoric and hydrostatic components of the form

$$S^d_{ij} = sY^d(s)\ E^d_{ij}$$

$$S^h_{kk} = sY^h(s)\ E^h_{ij}$$

where S and E denote stress and strain respectively. Subscripts indicate component directions with kk indicating summation of the 11, 22,

and 33 directions. Y(s) is the relaxation modulus corresponding to a particular reological model, and superscripts denote hydrostatic (h) or deviatoric (d) components. These equations can be combined to form the total stress equation

$$\sigma_{ij} = S^{d}_{ij} + \frac{1}{3}\delta_{ij} S^{h}_{ij}$$

where σ is the total stress and δ is the Kronecker delta.

For this study both the flesh and bone viscoelastic properties are modeled similarly. Figure 2 shows the three parameter deviatoric and simple elastic hydrostatic reological models used for either flesh or bone. The models are of the same form and differ only in parameter selection. Particular parameter selection will be discussed later in the results section. Using the correspondence principle, the finite element equations may now be developed in the Laplace domain similar to the methods used for the elastic case.

Bone Elements

Both the tibia and fibula are modeled using a series of ten beam elements, each of which is defined by eight displacement coordinates. Figure 3 shows a typical bone element along with its local, global, and displacement coordinate systems. Orne [7] determined that torsional effects as well as shear deformations have little effect on ulna response over the range of its first bending resonance. Assuming the same

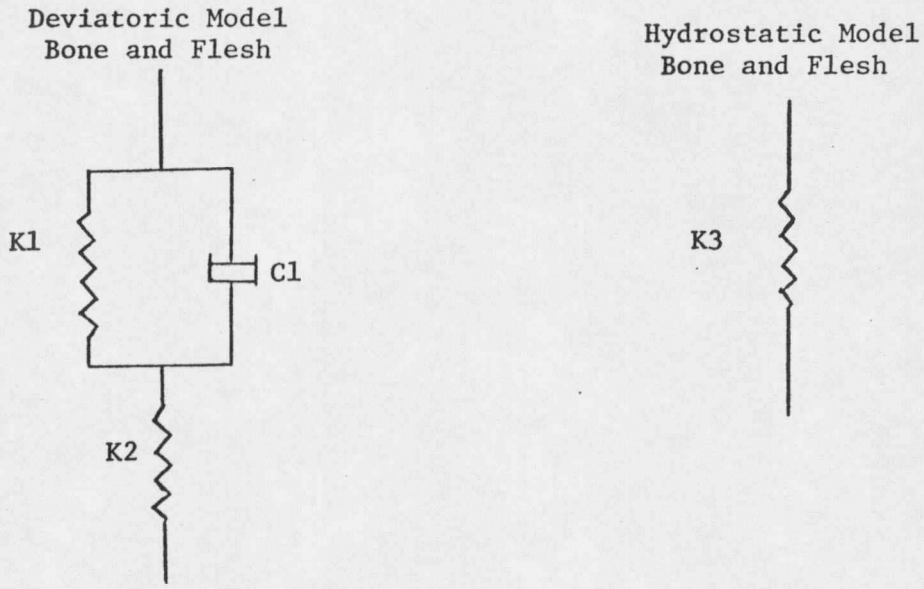

$$Y^d(s) = \frac{(B1 - B2)}{(B3 + s)} + \frac{B2}{s}$$

$$Y^h(s) = \frac{B4}{s}$$

where $B1 = K2$

$B2 = K1\ K2/(K1 + K2)$

$B3 = (K1 + K2)/C1$

$B4 = K3$

B1, B2, B3, and B4 are viscoelastic parameters for either flesh or bone, and are given values in later sections.

FIGURE 2.--Rheological Model

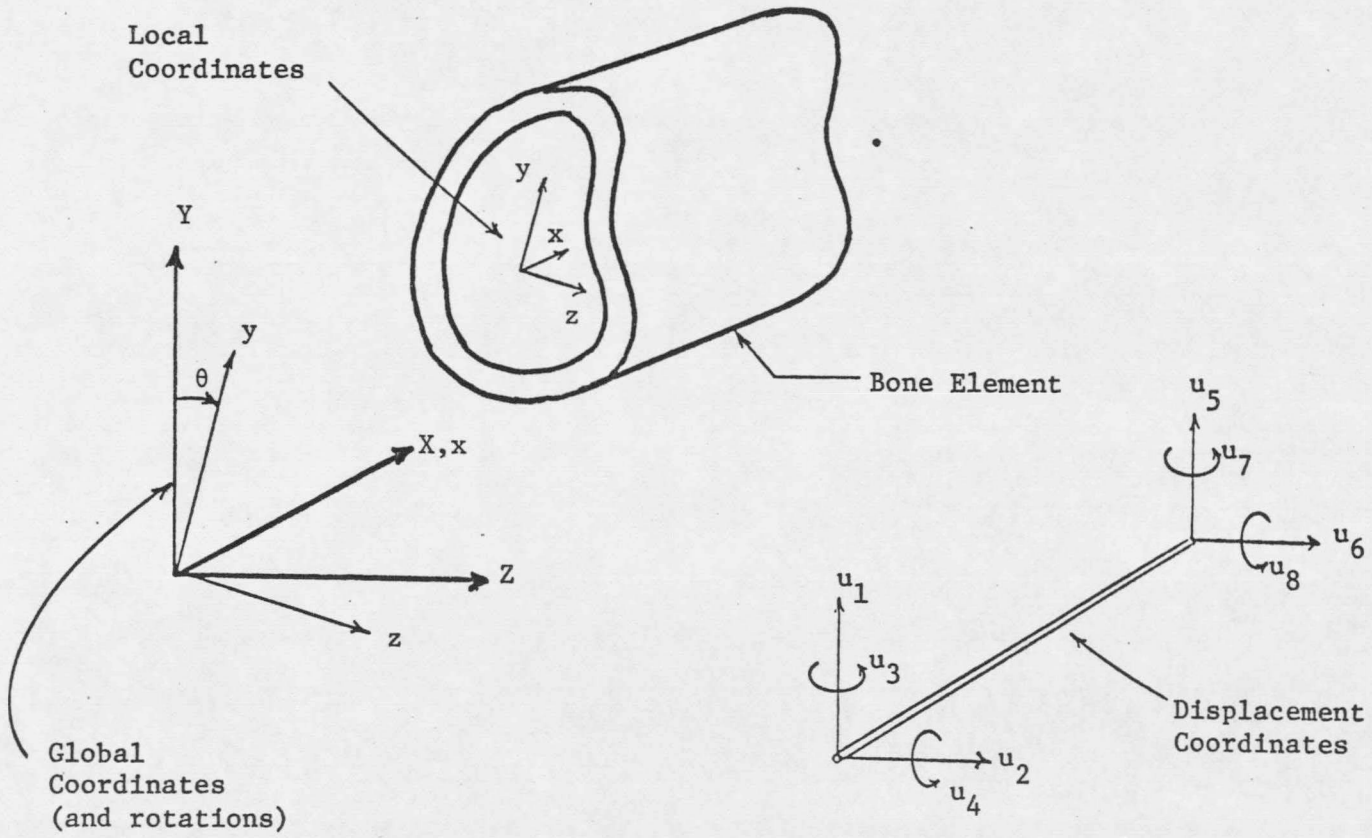

FIGURE 3.--Typical Beam Element

holds true for the tibia, and that deflection in the x direction (along the axis of the leg) is not important since transverse vibrational modes are dominant in the system, the standard beam element found in Przemieniecki [8] which requires twelve displacement coordinates is reduced to eight displacement coordinates. Figure 4 is a computer generated picture showing the twenty beam elements combined to form the bone structure of a typical right leg.

Geometric data from x-rays are used to determine the second moment of area about the principle major and minor axes as well as global coordinate rotations to those axes for each of the eleven cross sections defining each bone. Area and inertia are assumed to vary linearly with respect to distance along the element, resulting in stiffness and mass arrays that are somewhat different from those developed by Przemieniecki. These arrays and their derivation are described in Appendix I.

Flugge [9] has shown that the assumption of uniaxial stress for a beam allows simplification of the stress-strain relationships. A combined relaxation modulus, $Y^c(s)$, can be formed from deviatoric and hydrostatic relaxation moduli, and has the form

$$Y^c(s) = \frac{3\,Y^d(s)}{2 + Y^d(s)/Y^h(s)} \tag{3}$$

Thus, the viscoelastic bone stiffness array becomes

$$\underset{\sim}{K}_b(s) = sY^c(s)\,\underset{\sim}{K} \tag{4}$$

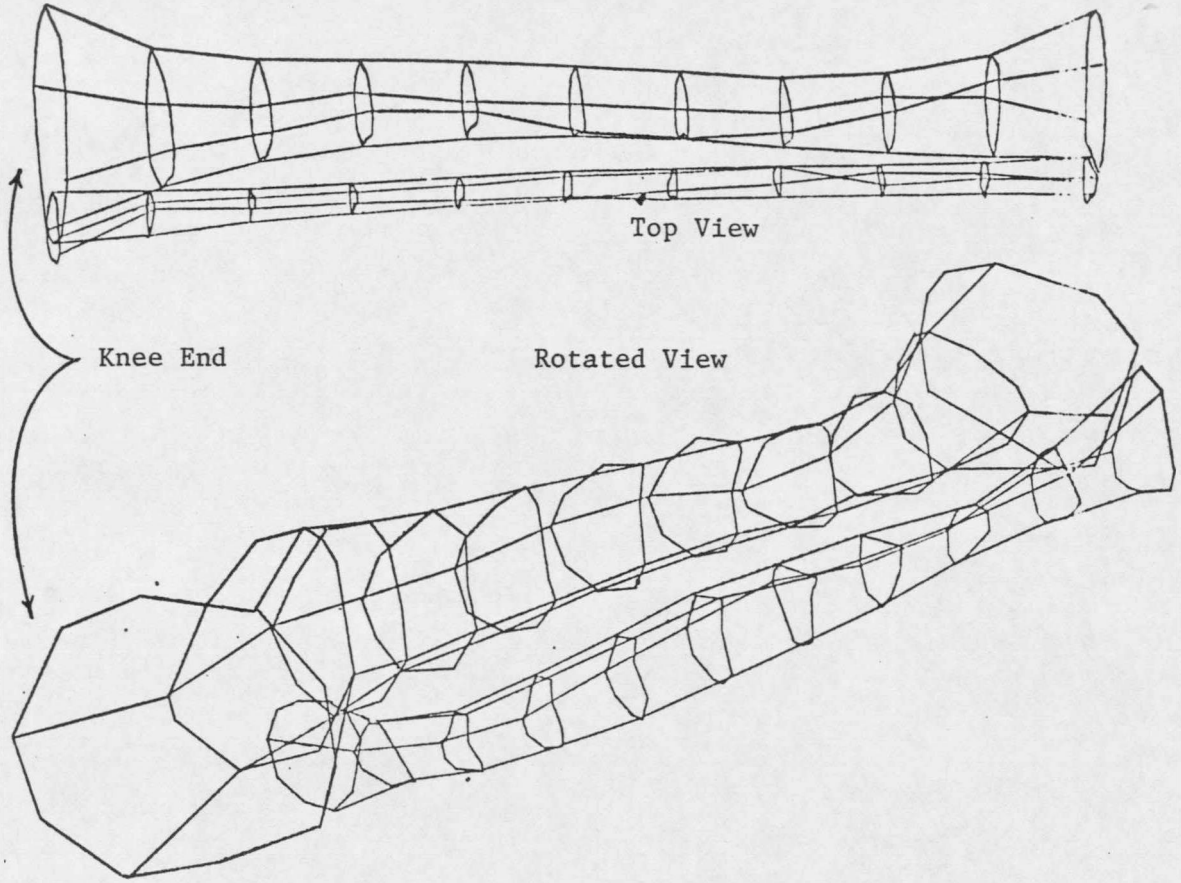

FIGURE 4.--Lower Leg Bone Structure

where $\underset{\sim}{K}$ is the bone stiffness array formed, as mentioned before, in Appendix I.

Flesh Elements

Flesh elements are lumped into two groups: collagenous tissue representing the interosseous ligament which runs between the tibia and fibula, and soft tissue representing the remainder of the surrounding flesh. Both groups are modeled using constant stress tetrahedron elements, with altered viscoelastic parameters accounting for their behavioral differences.

Referring to Figure 2, the interosseous ligament comprises the single hexahedron element between the tibia and fibula, with the remaining fourteen hexahedron elements comprising the soft tissue. Hexahedron elements are used because they are easy to visualize and construct, however, the computer forms the stiffness and mass arrays by breaking each hexahedron into five tetrahedrons and applying standard finite element methods to the tetrahedron elements. The tetrahedron mass and stiffness arrays are then properly combined forming the hexahedron arrays. Garner has developed the programming necessary to perform this operation as well as the theory and programming which splits these arrays into hydrostatic and deviatoric parts, therefore, the process will not be repeated here.

The combined flesh stiffness array, written in terms of hydrostatic and deviatoric arrays, has the form

$$\underset{\sim}{K}_f(s) = sY_1^d(s)\ \underset{\sim}{K}_{\sim 1}^d + sY_1^h(s)\ \underset{\sim}{K}_{\sim 1}^h + sY_2^d(s)\ \underset{\sim}{K}_{\sim 2}^d + sY_2^h(s)\ \underset{\sim}{K}_{\sim 2}^h \qquad (5)$$

where $\underset{\sim}{K}$ is a flesh geometric stiffness array with subscripts indicating soft (1) or collagenous (2) tissue types. The geometric stiffness arrays are independent of frequency and need only be formed once for a given model, resulting in considerable computer time savings if many runs are to be made changing only viscoelastic parameters.

Mode Reduction

Each of the eleven cross sections contains 23 flesh nodes, and 2 bone nodes. Each flesh node has three coordinate directions while each bone node has four coordinate directions, combining to form 77 displacement coordinates for each cross section or 847 displacement coordinates for the total system. Therefore, solving Equation 2 for $\underline{u}(j\omega)$ involves the solution of 847 simultaneous complex equations for each given frequency. Generation of a response plot requires numerous such solutions for $\underline{u}(j\omega)$ depending on the bandwidth of the plot and the spacing between frequency points. For this study, 50 points are generated, producing a plot with frequencies ranging from 0-1000 hertz. Solving Equation 2 using standard simultaneous equation routines available on a computer is impractical, and other means of solution must be sought. Fortunately,

the bandwidth of the response is limited and reduction of the system arrays can be accomplished using the method of assumed modes, sometimes referred to as Galerkin's method [10]. The method involves reducing the degress of freedom of a system by using a set of assumed displacement mode shapes. Displacement coordinates are related to a set of reduced generalized coordinates by the matrix equation

$$\underline{U}(j\omega) = \underset{\sim}{\gamma}\underline{P}(j\omega) \tag{6}$$

where $\underset{\sim}{\gamma}$ = n x m mode shape array,

n = number of displacement coordinates,

m = number of assumed modes, and

$\underline{P}(j\omega)$ = vector of reduced generalized coordinates.

This study assumes 18 independent sinusoidal and rigid body bone modes and 9 independent flesh modes, totaling 27 independent mode shapes. The reduced equations now take the form

$$\underset{\sim}{D}_r(j\omega)\,\underline{P}(j\omega) = \underline{F}_r(j\omega) \tag{7}$$

where $\underset{\sim}{D}_r(j\omega) = (-\omega^2 \underset{\sim}{\gamma}^t \underset{\sim}{M} \underset{\sim}{\gamma} + \underset{\sim}{\gamma}^t \underset{\sim}{K}_b(j\omega) \underset{\sim}{\gamma} + \underset{\sim}{\gamma}^t \underset{\sim}{K}_f(j\omega) \underset{\sim}{\gamma}]$, and

$\underline{F}_r(j\omega) = \underset{\sim}{\gamma}^t \underline{F}(j\omega)$.

The reduced system arrays are now 27 x 27 and are easily handled using a computer. Solving Equation 7 for $\underline{P}(j\omega)$ and substitution into Equation 6 yields coordinate displacement amplitudes.

CHAPTER III

RESULTS

The following section describes several response tests performed on a single model developed from a pair of x-rays received from the student health center at Montana State University. The tests show the effects of altering various bone, flesh, and end condition viscoelastic parameters, and are compared with experimental data.

The patient of whom the x-rays were taken was not available for experimental tests, hence, no exact tissue properties could be determined. However, experimental response plots of several test subjects showed marked similarities, and generalized comparisons between theoretical and analytical response plots could be made. The primary objectives of these tests are to verify the accuracy of the model and demonstrate its usefulness, both of which can be accomplished with these single model tests.

Flugge [9] has shown that for the case of uniaxial stress, an equivalent Young's modulus (E) and Poisson's ratio (ν) can be written

$$E = sY^{c}(s)$$

$$\nu = \frac{Y^{h}(s) - Y^{d}(s)}{2Y^{h}(s) + Y^{d}(s)}$$

Both E and ν are shown in Table 1 along with the bone parameters for the eight test runs. Tables 2 and 3 show soft and collagenous tissue viscoelastic properties for the same eight tests. Input and output trans-

TABLE 1.--Bone Properties

Run #	B1 (GPa)	B2 (GPa)	B3 (sec^{-1})	B4 (GPa)	E (GPa)	ν
1	68.9	13.2	1×10^8	43.1	17.2	.3
2	27.6	15.92	1×10^8	51.7	20.7	.3
3	27.6	15.92	2×10^4	51.7	20.7	.3
4	27.6	15.92	2×10^4	51.7	20.7	.3
5	27.6	15.92	2×10^4	51.7	20.7	.3
6	27.6	15.92	2×10^4	51.7	20.7	.3
7	27.6	15.92	2×10^4	51.7	20.7	.3
8	27.6	15.92	2×10^4	51.7	20.7	.3

TABLE 2.--Flesh Properties

Run #	B1 (GPa) $\times 10^4$	B2 (GPa) $\times 10^7$	B3 (sec^{-1})	B4(GPa) $\times 10^7$
1	--	--	--	--
2	--	--	--	--
3	--	--	--	--
4	3.65	3.45	10^8	12.4
5	3.65	3.45	10^8	12.4
6	3.65	3.45	10^8	12.4
7	3.65	3.45	6000	12.4
8	3.65	3.45	6000	12.4

TABLE 3.--Interosseous Ligament Properties

Run #	B1 (GPa) x 10^4	B2 (GPa) x 10^7	B3 (sec^{-1})	B4 (GPa) x 10^7
1	--	--	--	--
2	--	--	--	--
3	--	--	--	--
4	3.65	3.45	10^8	12.4
5	3.65 x 10^3	3.45 x 10^3	10^8	12.4 x 10^3
6	3.65	3.45	10^8	12.4
7	3.65	3.45	6000	12.4
8	3.65	3.45	6000	12.4

ducer locations for experimental and model tests are shown in Figure 5 and a summary of these runs is listed in Table 4.

Test runs 1 through 3 are response tests performed on just the tibia, excluding the effects of the fibula and flesh. The first two tests demonstrate the effect of increasing the static viscoelastic equivalent Young's modulus from 17 Gpa (test 1) to 20 Gpa (test 2) while holding Poisson's ratio at .3 and damping to zero. Both values of Young's modulus fall within the range of values reported by several sources [11, 12, 13]. Since tests 1 and 2 include no damping, their viscoelastic properties may be completely defined by specifying E and ν. For the third test damping is added to the test 2 undamped model.

The remaining five tests show the influence of flesh and end condition stiffness on the bone structure described by test 3. For those tests, the elastic and viscoelastic flesh parameters are those determined by Garner [6]. Undamped and damped flesh parameters are added to the system for runs 4 and 7 respectively. In test 5, interosseous ligamental material properties, which had previously been held to values representing the surrounding flesh, were stiffened. End condition stiffness was relaxed for test 6 to allow rigid body motion, and the final test run combines several of the previous tests into a single run.

Figures 6, 7, and 8 show the analytical results of the first two test runs, and a typical experimental response plot. Experimental procedures involve strapping an accelerometer to the leg for output measure-

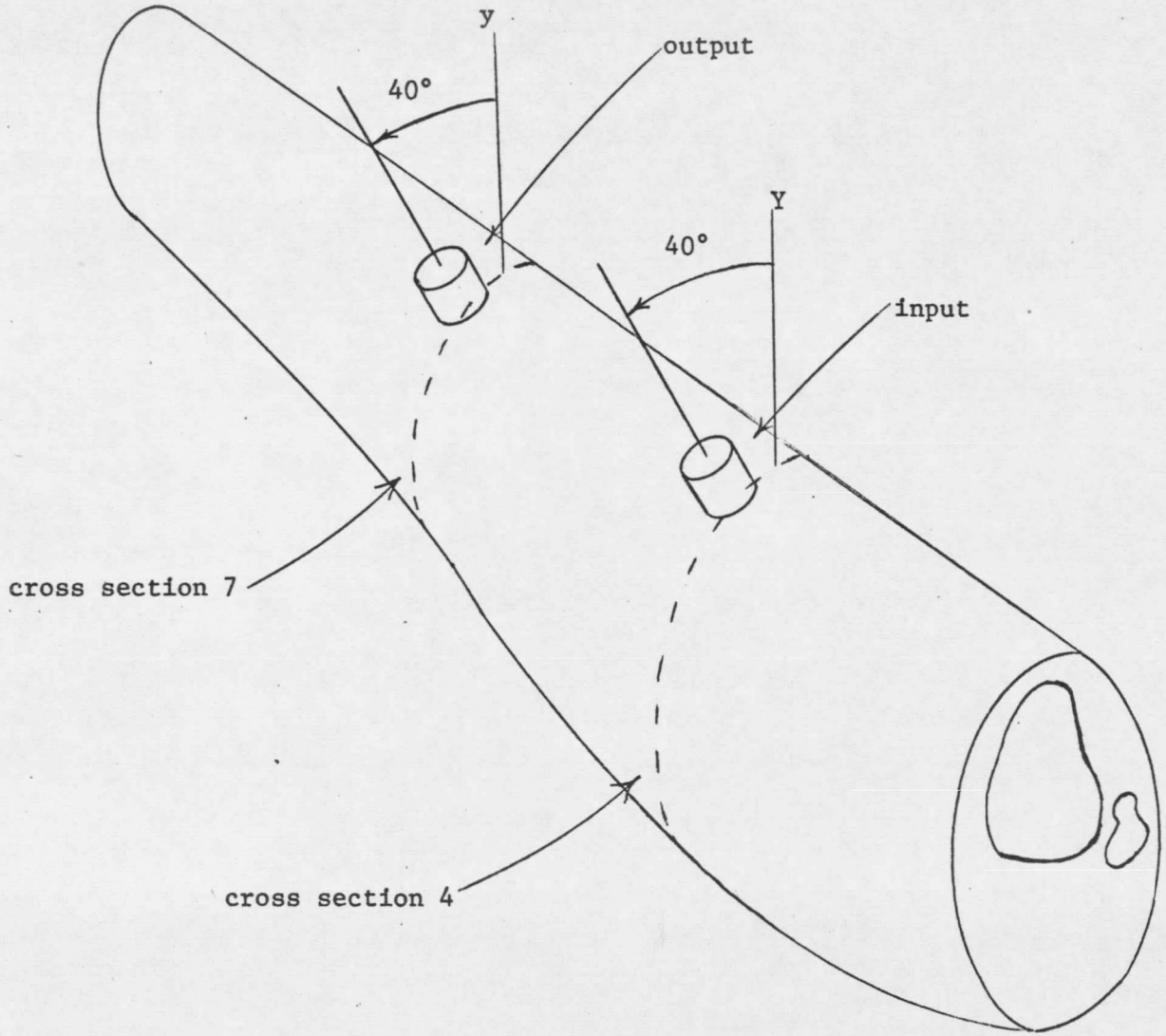

FIGURE 5.--Transducer Locations (Right Leg)

TABLE 4.--Summary of Runs

Run	Bone	Flesh	Interosseous Ligament	End Condition
1	undamped	none	none	pinned
2	undamped	none	none	pinned
3	damped	none	none	pinned
4	damped	undamped	loose	pinned
5	damped	undamped	tight	pinned
6	damped	undamped	loose	elastic
7	damped	damped	loose	pinned
8	damped	damped	tight	elastic

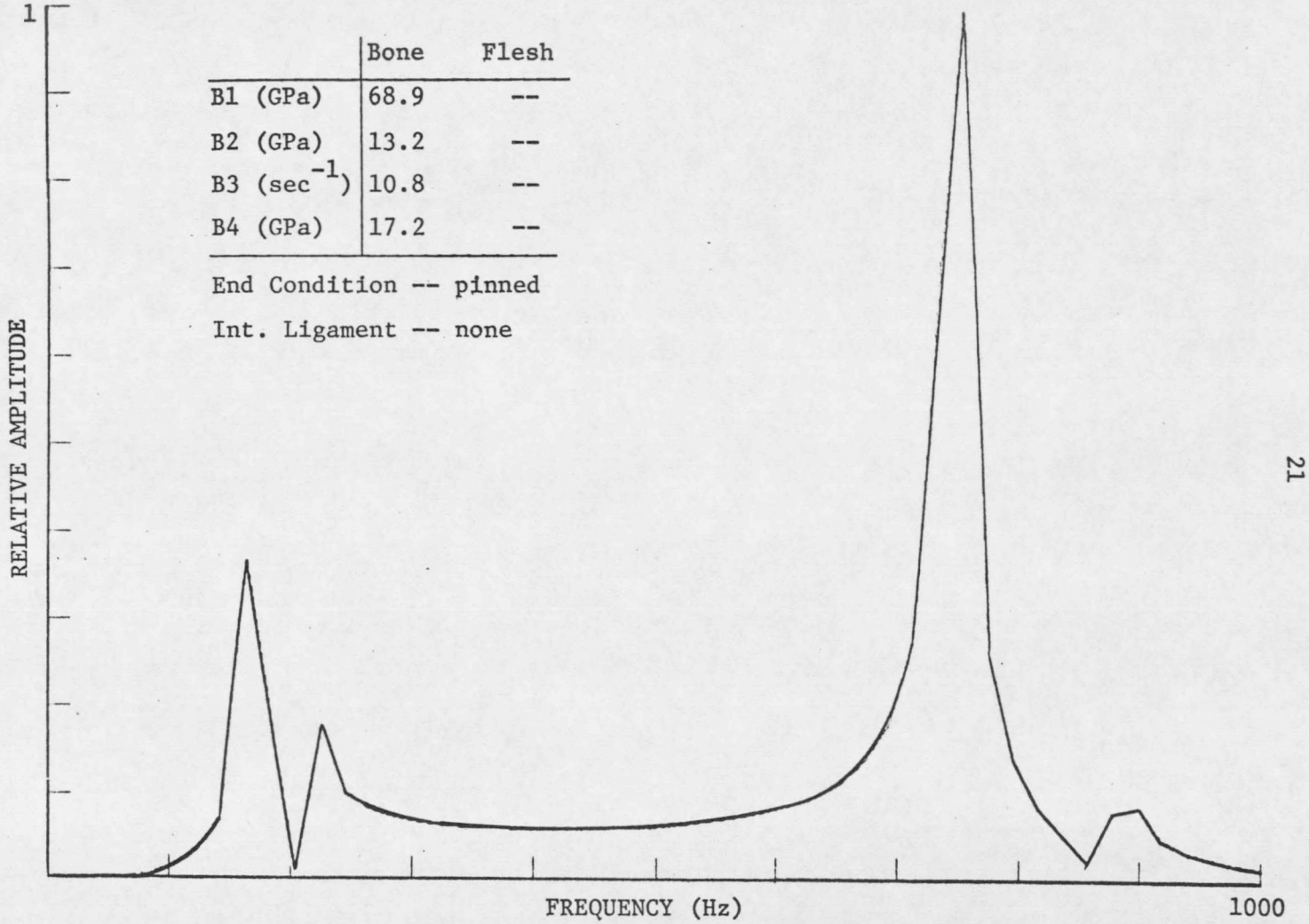

FIGURE 6.--Response Plot (Run 1)

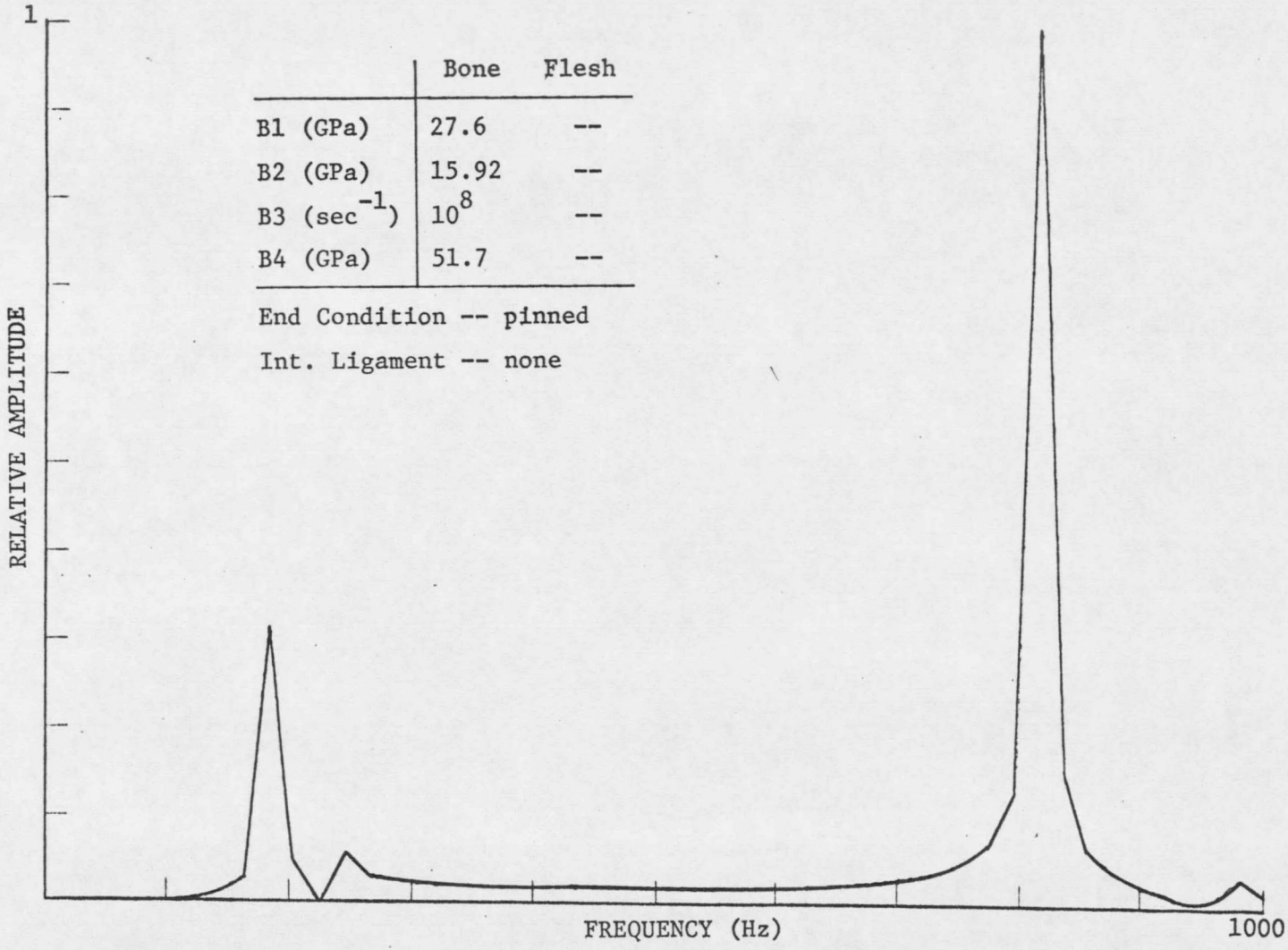

FIGURE 7.--Response Plot (Run 2)

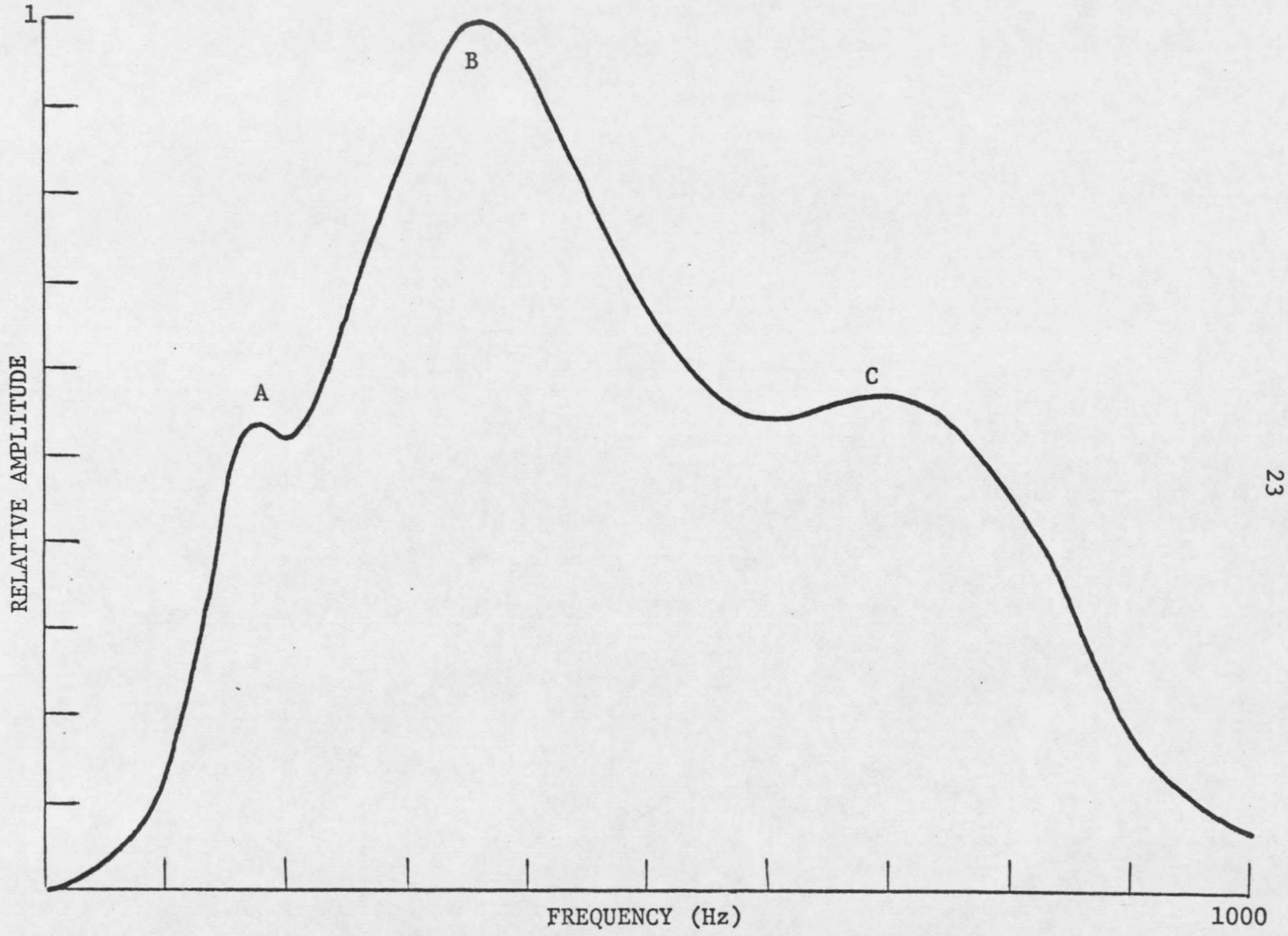

FIGURE 8.--Response Plot (Experimental)

ments, and exciting the leg using an electromagnetic shaker. For details of this type of testing, see Harrigan [14]. Results show that output response is dependent upon the amount of pressure applied by the accelerometer, and repeatable results are difficult to obtain because of the flesh interface between the accelerometer and bone. However, all tested subjects had the three peaks A, B, and C common to their response plots (see Figure 8). Although the experimental plot looks considerably different than the analytical plots, note that the relative locations of the first three natural frequency peaks tend to match. Further analytical and experimental tests indicate the first two peaks represent the first bending mode of vibration in two planes (see Figure 9) while the third peak represents the second bending natural frequency. As expected, the increased stiffness from run 1 to 2 increases the natural frequencies of the system.

The results of adding damping to the test 2 model are shown in Figure 10. Note that the proportional size of the amplitude peaks tend to match experimental data. Non-linear damping with respect to frequency is obtainable using the 3 parameter solid model, and therefore, the relative size between first and second resonance frequency peaks can be adjusted by altering the damping and stiffness parameters.

Figure 11 illustrates response of test 4 and indicates that the addition of undamped flesh has little effect other than lowering the system natural frequencies. This is expected since considerable mass is

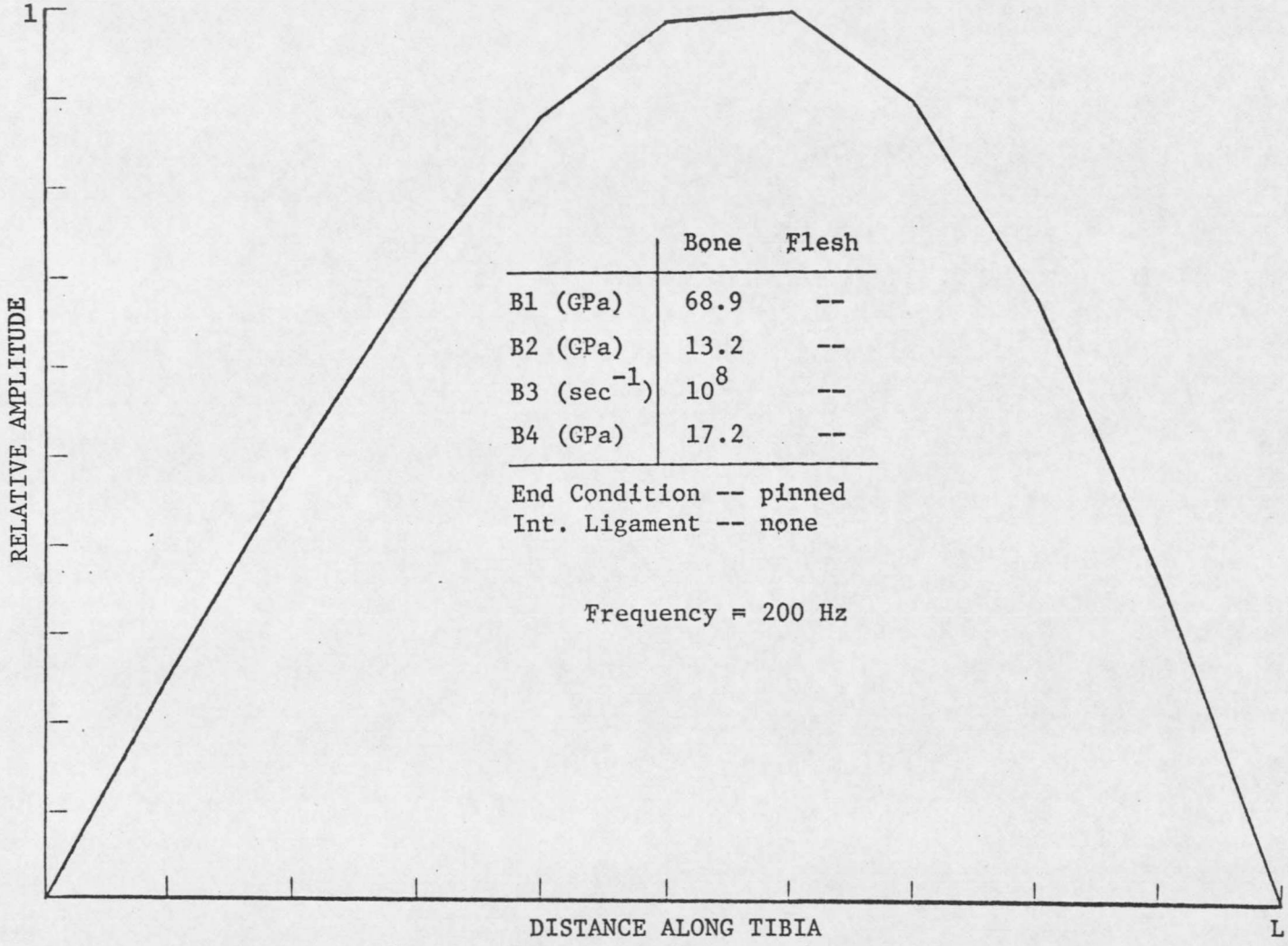

FIGURE 9.--Mode Diagram (Run 1)

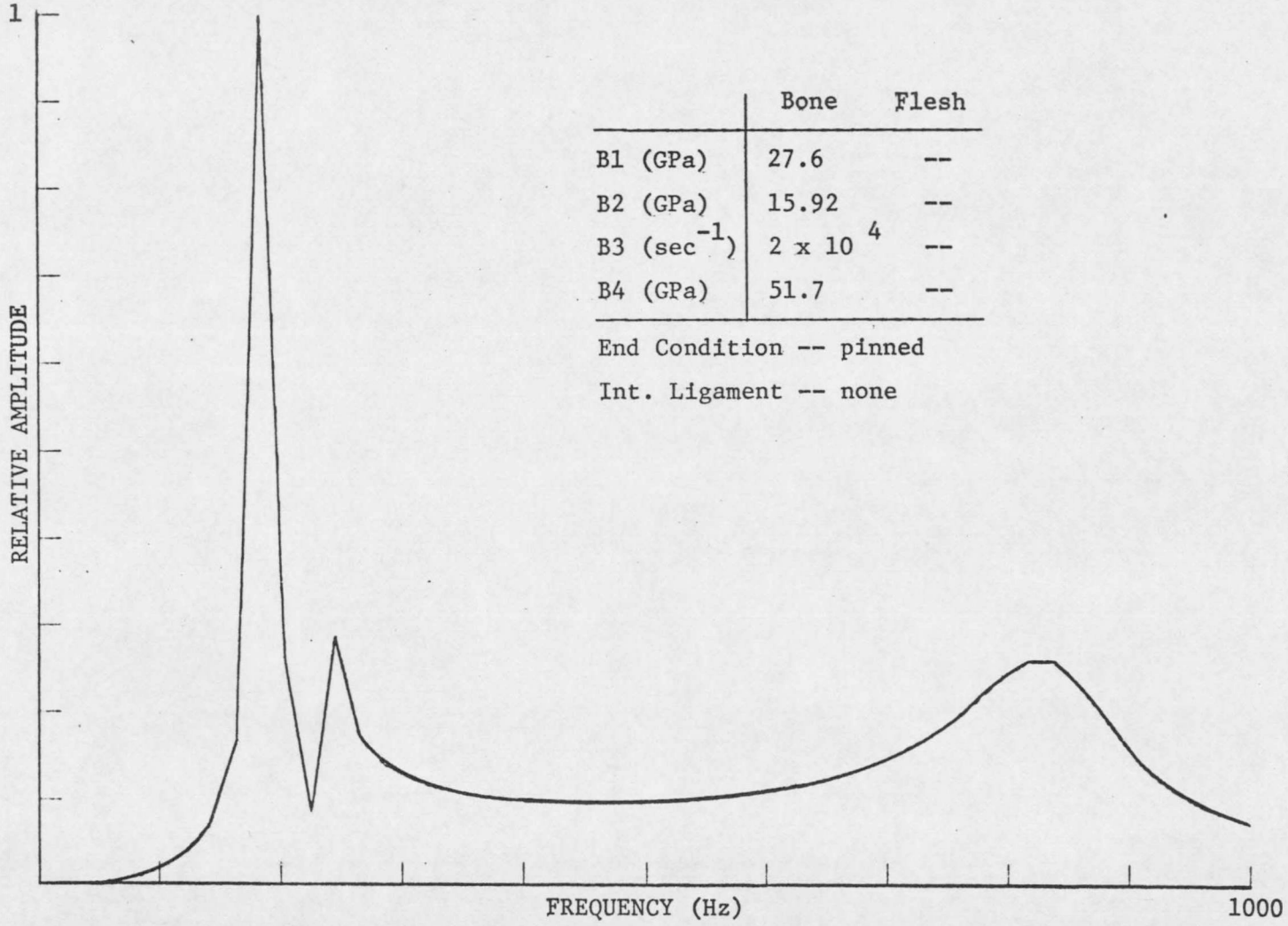

	Bone	Flesh
B1 (GPa)	27.6	--
B2 (GPa)	15.92	--
B3 (sec^{-1})	2×10^4	--
B4 (GPa)	51.7	--

End Condition -- pinned

Int. Ligament -- none

FIGURE 10.--Response Plot (Run 3)

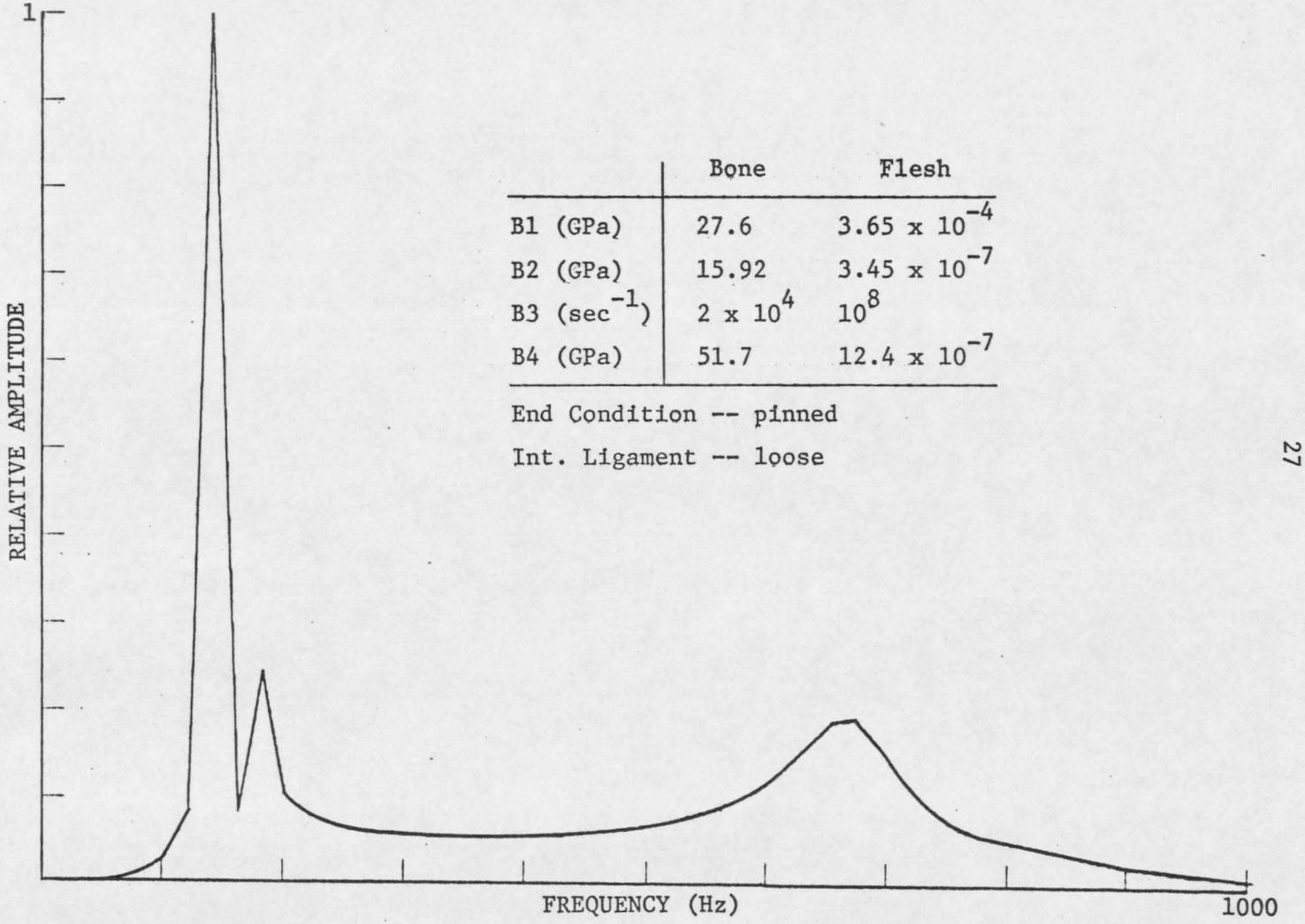

	Bone	Flesh
B1 (GPa)	27.6	3.65×10^{-4}
B2 (GPa)	15.92	3.45×10^{-7}
B3 (sec^{-1})	2×10^{4}	10^{8}
B4 (GPa)	51.7	12.4×10^{-7}

End Condition -- pinned

Int. Ligament -- loose

FIGURE 11.--Response Plot (Run 4)

being added to the system. On the other hand, increasing the interosseous ligament stiffness (test 5, Figure 12) has a marked effect on system response. Increasing this stiffness would tend to increase the role of the fibula response, and indeed a third peak is added to the first bending mode group.

The response plot and mode shape diagram for run 6 are shown in Figures 13 and 14. The results of this test indicate a lowering of the second natural frequency of the system. This might be expected since some rigid body motion is being coupled into the bending vibrational modes, and is important since experimental plots tend to show this relationship between first and second modes of vibration.

Run 7, Figure 15, shows that damped flesh tends to lower the relative amplitude of the first bending mode with respect to the second bending mode, raise the relative height of the second peak in the first natural frequency group, and generally broaden the response peaks. All of these results are significant, however, not necessarily unexpected.

The final run is significant in that it tends to resemble experimental results (Figure 16). Since this run includes flesh damping, loosened end condition stiffness, and a stiffened interosseous ligament, it indicates that possibly all of these factors have an affect on the system response for the actual case.

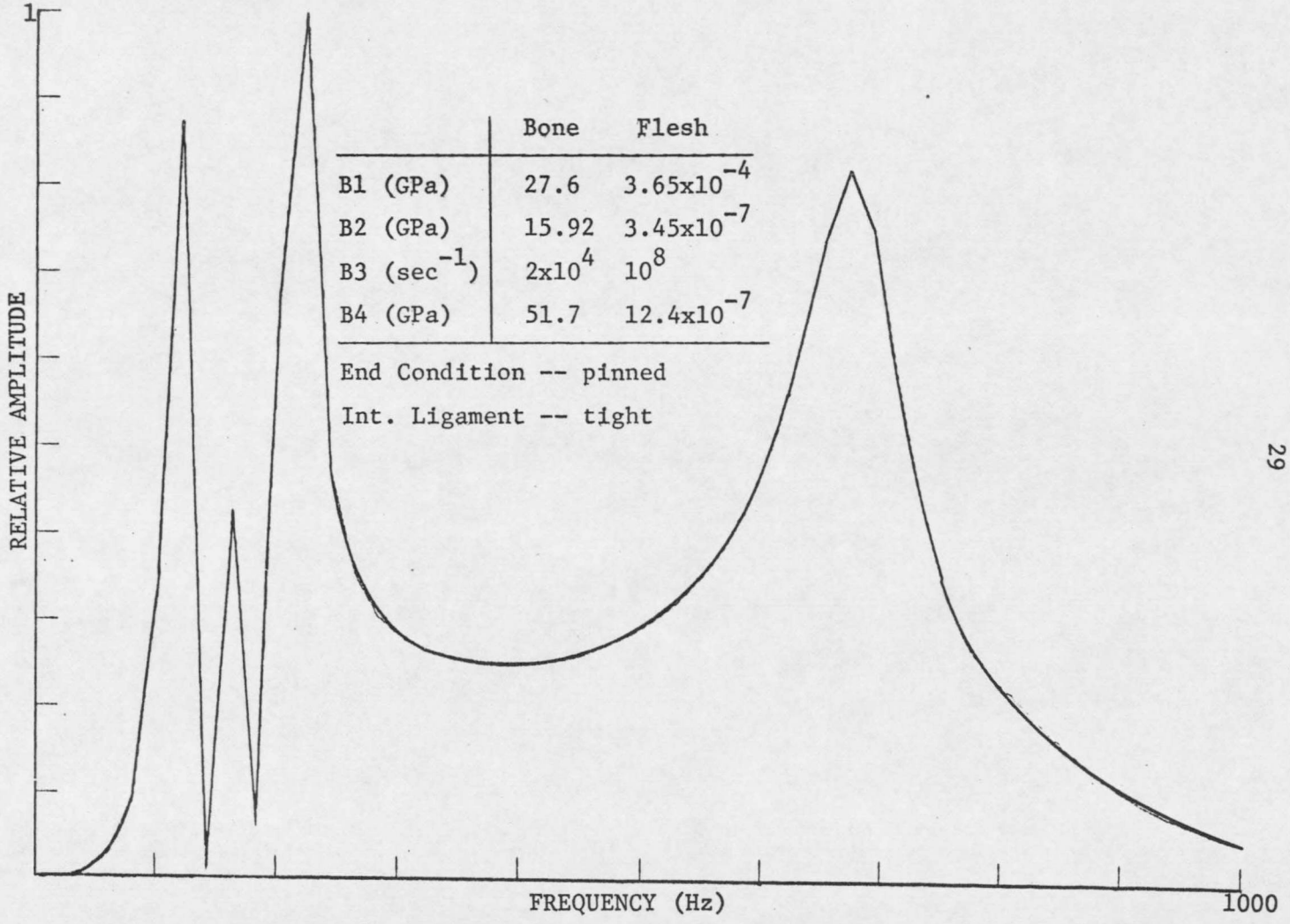

FIGURE 12.--Response Plot (Run 5)

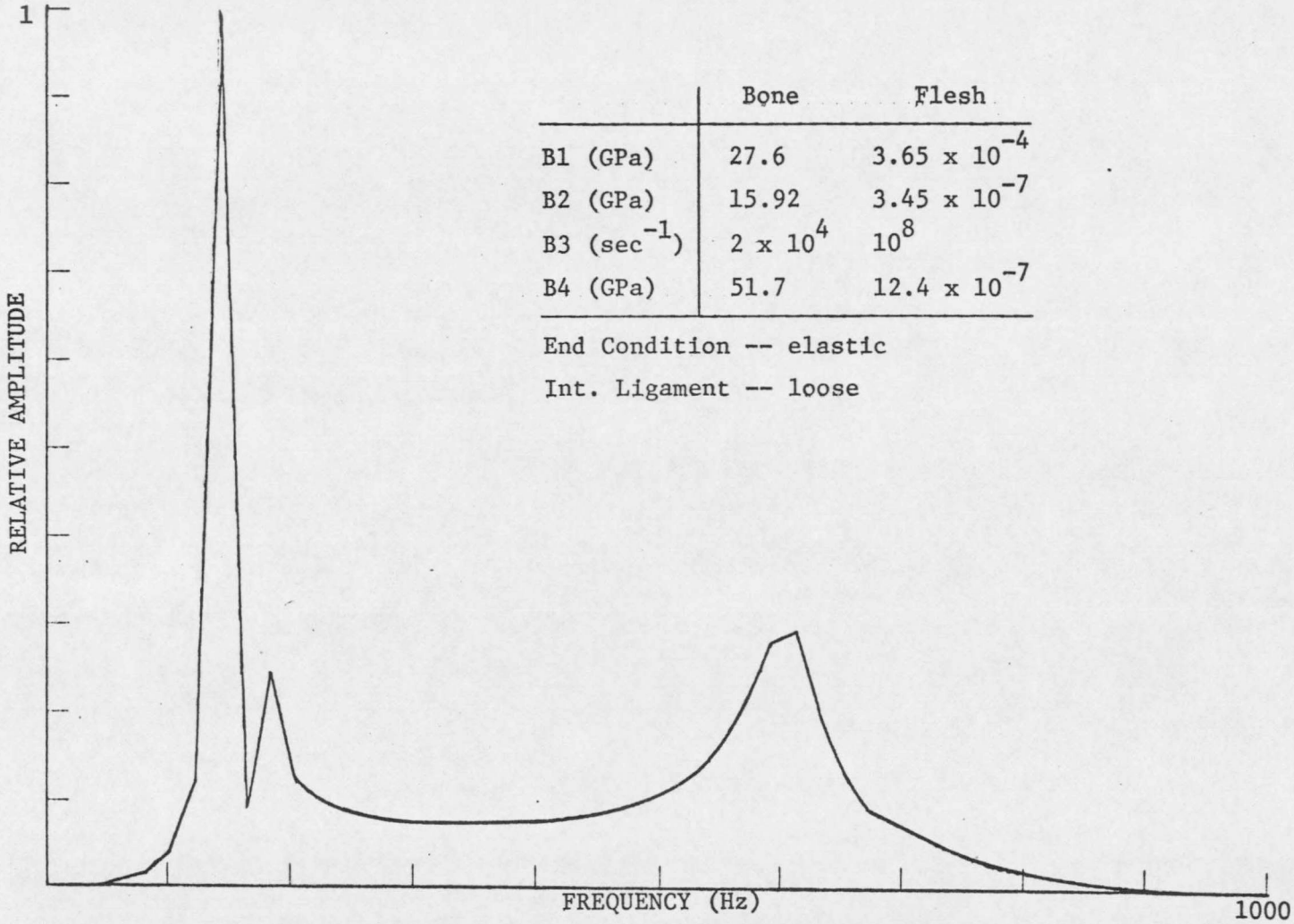

	Bone	Flesh
B1 (GPa)	27.6	3.65×10^{-4}
B2 (GPa)	15.92	3.45×10^{-7}
B3 (sec^{-1})	2×10^{4}	10^{8}
B4 (GPa)	51.7	12.4×10^{-7}

End Condition -- elastic

Int. Ligament -- loose

FIGURE 13.--Response Plot (Run 6)

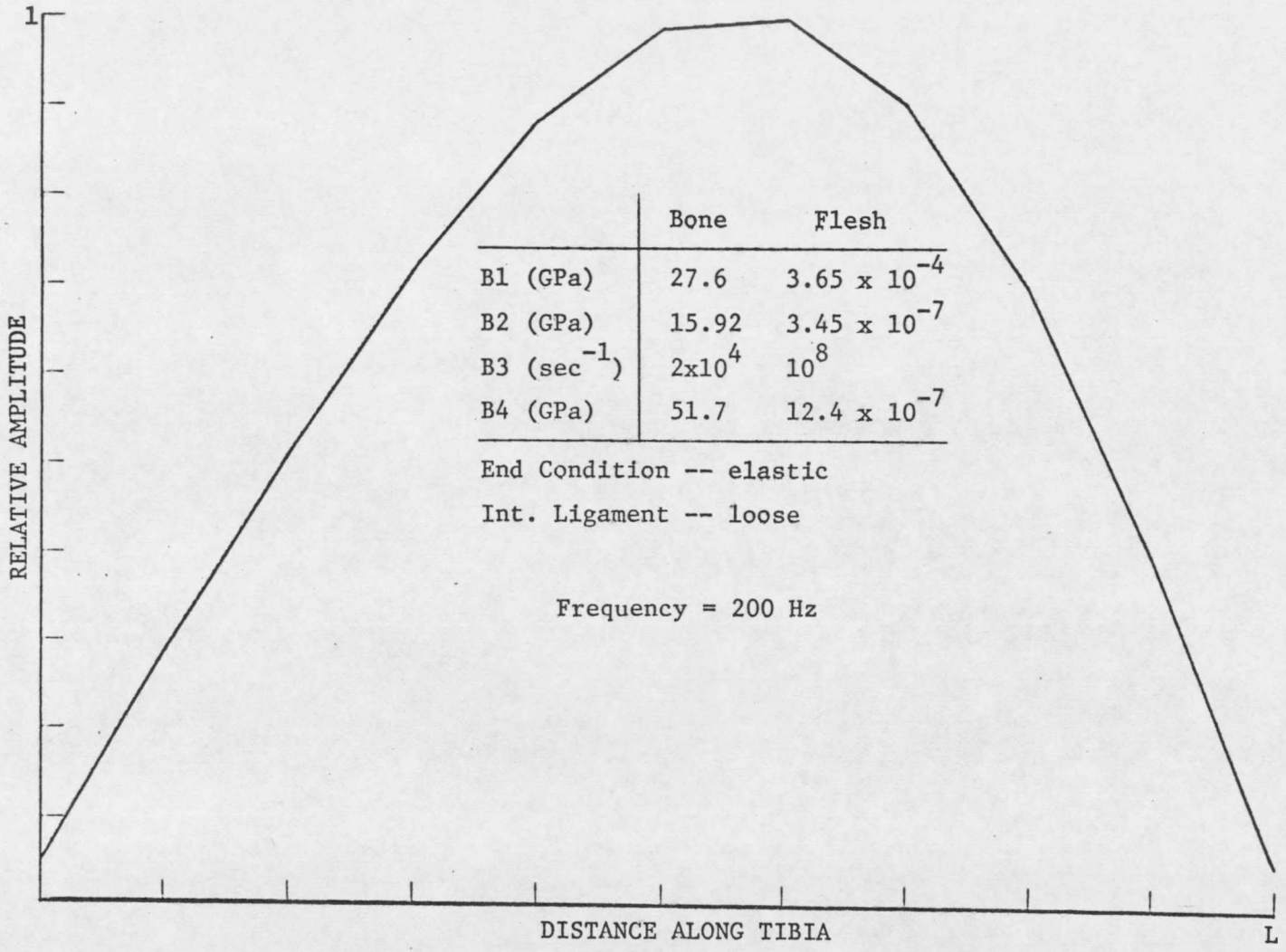

FIGURE 14.--Mode Diagram (Run 6)

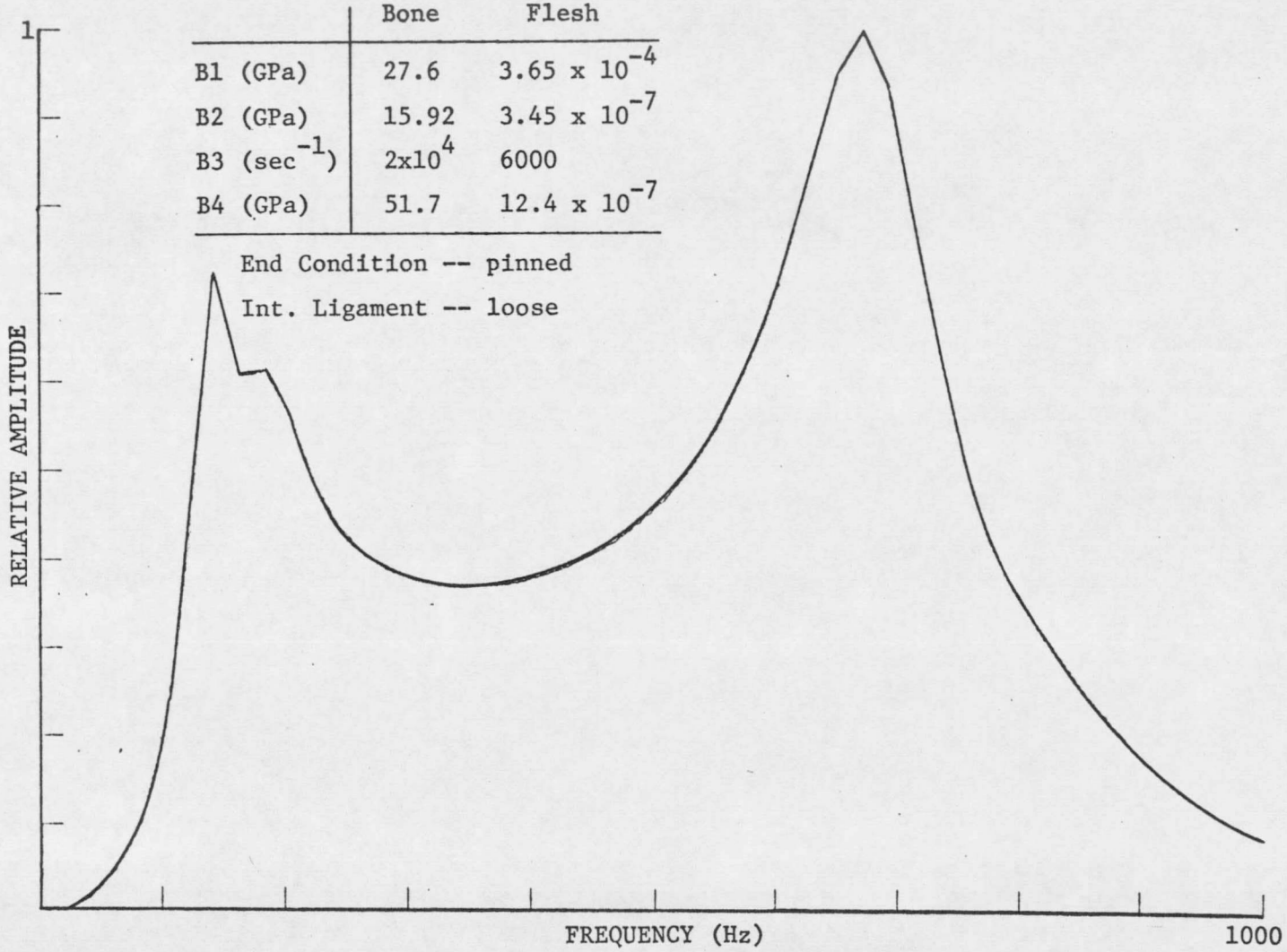

FIGURE 15.--Response Plot (Run 7)

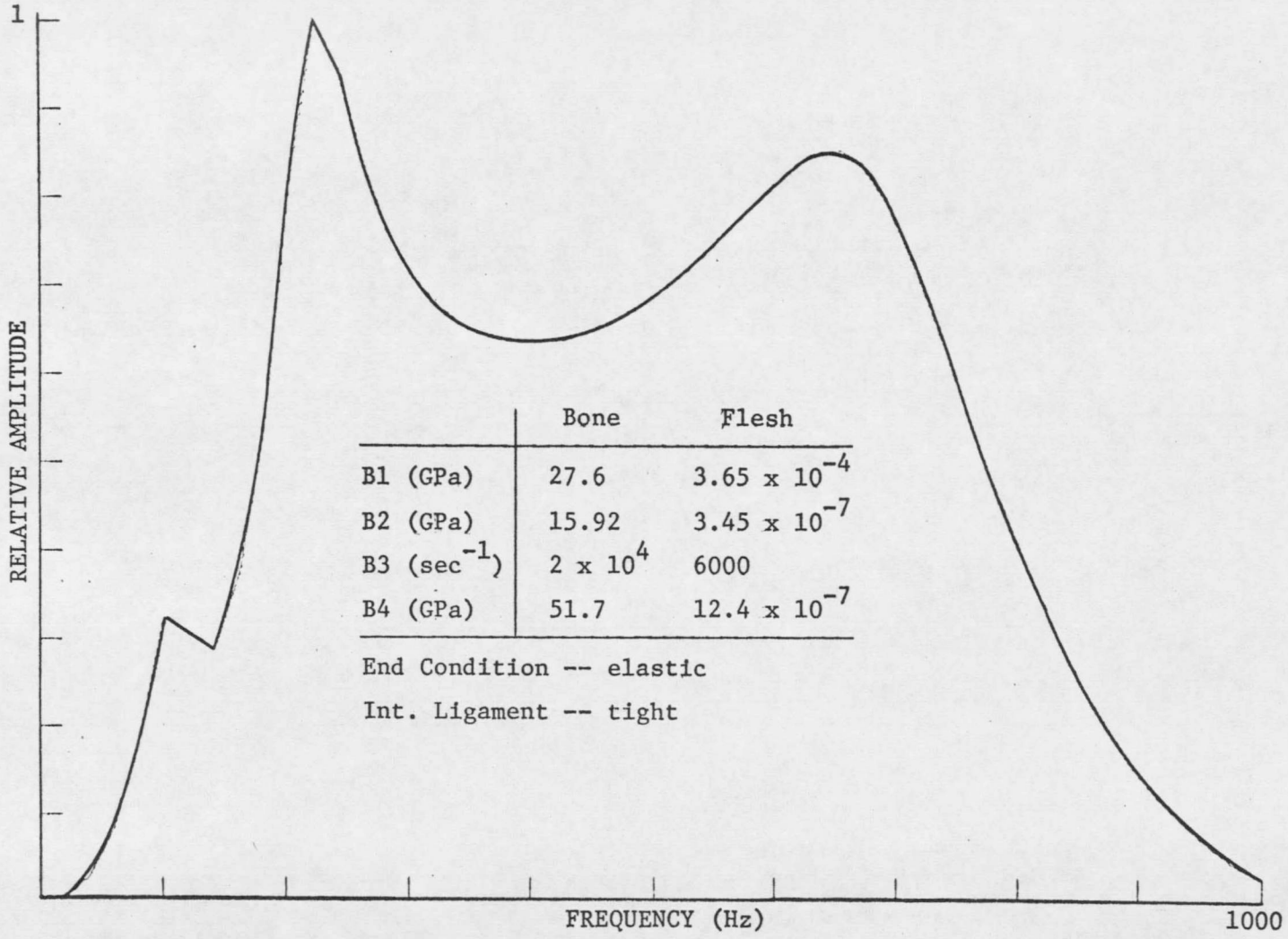

FIGURE 16.--Response Plot (Run 8)

CHAPTER IV

CONCLUSION

The intent of this study was to construct a model which will simulate the dynamic response of the lower human leg subject to harmonic excitation.

The eight test response runs in the previous section show the contributions of several of the bone and flesh parameters. Adjustments of these parameters can be made such that the analytical response curve can be forced to a near fit of experimental plots. Thus, there is the potential for defining material properties in terms of the analytical proceedures presented here, when they are correlated with experimental results. The results also indicate that the acceleration peaks measured by Jurist and others are indeed those excited by bone bending modes of vibration. Perhaps even more significant is the fact that these plots tend to show that interosseous ligament stiffness, end condition stiffness, and flesh damping have a mojor effect on the system response. These facts indicate that vibrational methods of measuring bone stiffness may not be practical due to the interactions of the bone with surrounding ligaments. On the other hand, comparisons concerning the contributions of several of the tested parameters might be misleading since the experimental response plots were generated using unsophisticated equipment, and were not created for the purpose of obtaining accurate tissue mechanical properties. Analysis confirms that proper selec-

tion of viscoelastic bone and flesh parameters will yield analytical results which match experimental data.

The author wishes to emphasize the need for improved test equipment. Accurate tissue properties can only be derived using test equipment which can accurately measure the response of the human leg. There is also a need for test equipment capable of determining which modes of vibration are being excited. With improved test equipment, several patients, from whom accurate models can be constructed, should be tested. The results of these tests can then be used to statistically verify whether or not bone vibrational measurements can prove to be a useful tool.

As a final comment, it appears that considerable work is still necessary in the area of long bone vibration testing. Better testing techniques used in conjunction with sophisticated models, such as the one presented here, could prove to be an aid to many areas of medical diagnostics.

APPENDIX I

MASS AND STIFFNESS ARRAYS

This appendix describes the derivation of the mass and stiffness arrays used for this study.

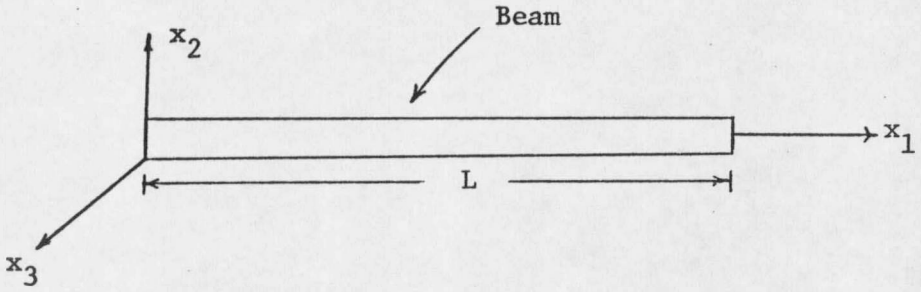

x_1 = centroidal axis

x_2 = principle minor axis

x_3 = principle major axis

The strain energy (U_s) of a beam in bending (x_2 direction) is

$$U_s = \int_o^L \frac{1}{2} EI(x_1)[\mu''(x_1)]^2 dx_1 \qquad \text{(I-1)}$$

where E = Young's Modulus (assumed constant with respect to x_1),

$I(x_1)$ = Second moment of area about x_3, and

$\mu(x_1)$ = Displacement of the beam in the x_2 direction (Primes indicate derivatives with respect to x_1).

Assuming $\mu(x_1)$ can be written as a cubic equation in x_1

$$\mu(x_1) = a_0 + a_1 x_1 + a_2 x_1^2 + a_3 x_1^3 \qquad \text{(I-2)}$$

Then $\mu(x_1)$ can be written in terms of the displacement coordinates u_1, u_4, u_5, and u_8 (see Figure 3) by solving for the unknowns (a_0, a_1, a_2, a_3) in terms of the displacement coordinates. The resulting set of equations are

$$\begin{pmatrix} a_0 \\ a_1 \\ a_2 \\ a_3 \end{pmatrix} = \begin{pmatrix} 1 & 0 & 0 & 0 \\ 0 & 1 & 0 & 0 \\ 1 & L & L^2 & L^3 \\ 0 & 1 & 2L & 3L^2 \end{pmatrix} = \begin{pmatrix} u_1 \\ u_2 \\ u_3 \\ u_4 \end{pmatrix} \tag{I-3}$$

If $I(x_1)$ is a linear function of x_1 and can be written

$$I(x_1) = \frac{I(L) - I(0)}{L} x_1 + I(0)$$

then equation I-1 becomes

$$U_s = \frac{1}{2} E \left[I(L) \int_0^L x_1 [\mu''(x_1)]^2 dx_1 + I(0) \int_0^L (1-x_1)[\mu''(x_1)]^2 dx_1 \right] \tag{I-4}$$

Substituting Equations I-2 and I-3 into Equation I-4 yields a strain energy matrix equation in terms of the displacement vector $\underline{U}$

$$U_s = \frac{1}{2} E \, \underline{U}^t \underset{\sim}{K} \underline{U} \tag{I-5}$$

where $\underline{U}^t = [u_1, u_4, u_5, u_8]$,

and $\underset{\sim}{K}$ is a 4 x 4 stiffness array that is a function of element length and end inertias.

Expanding this procedure to three dimensions (allowing bending in

both the x_2 and x_3 directions) produces a set of 8 simultaneous equations in the same form as Equation I-5 where the displacement vector now becomes

$$\underline{U}^t = [u_1, u_2, u_3, u_4, u_5, u_6, u_7, u_8]$$

Mass array development follows along similar lines by assuming area is a linear function of x_1. Then the kinetic energy equation

$$T = \int_0^{L_1} \frac{1}{2} \rho A(x_1) [\dot{u}(x_1)]^2 dx_1$$

can then be solved in terms of $\dot{\underline{U}}$ and has the form

$$T = \frac{1}{2} \dot{\underline{U}}^t \underset{\sim}{M} \dot{\underline{U}} \qquad \text{(I-6)}$$

where T = kinetic energy,

$\dot{\underline{U}} = [\dot{u}_1\ \dot{u}_2\ \dot{u}_3\ \dot{u}_4\ \dot{u}_5\ \dot{u}_6\ \dot{u}_7\ \dot{u}_8]$, (dots indicate derivatives with respect to time),

$\underset{\sim}{M}$ = consistent mass matrix, and

ρ = mass density.

Equations I-5 and I-6 are the basic energy equations used in finite element analysis. Figure I-1 shows the complete mass ($\underset{\sim}{M}$) and stiffness ($\underset{\sim}{K}$) arrays used for this study. Looking at these arrays there are two interesting things to note: First, the arrays are functions of geometry and density only. Young's modulus is independent of these arrays, and

$$
\underset{\sim}{K} = \begin{bmatrix}
\frac{6I_3(0)}{\ell^3} & & & & & & & \\
0 & \frac{6I_2(0)}{\ell^3} & & & & & & \\
0 & -\frac{4I_2(0)}{\ell^2} & \frac{3I_2(0)}{\ell} & & & \text{Symmetric} & & \\
\frac{4I_3(0)}{\ell^2} & 0 & 0 & \frac{3I_3(0)}{\ell} & & & & \\
-\frac{6I_3(0)}{\ell^3} & 0 & 0 & -\frac{4I_3(0)}{\ell^2} & \frac{6I_3(0)}{\ell^3} & & & \\
0 & -\frac{6I_2(0)}{\ell^3} & \frac{4I_2(0)}{\ell^2} & 0 & 0 & \frac{6I_2(0)}{\ell^3} & & \\
0 & -\frac{2I_2(0)}{\ell^2} & \frac{I_2(0)}{\ell} & 0 & 0 & \frac{2I_2(0)}{\ell^2} & \frac{I_2(0)}{\ell} & \\
\frac{2I_3(0)}{\ell^2} & 0 & 0 & \frac{I_3(0)}{\ell} & -\frac{2I_3(0)}{\ell^2} & 0 & 0 & \frac{I_3(0)}{\ell}
\end{bmatrix} + \begin{bmatrix}
\frac{6I_3(\ell)}{\ell^3} & & & & & & & \\
0 & \frac{6I_2(\ell)}{\ell^3} & & & & & & \\
0 & -\frac{2I_2(\ell)}{\ell^2} & \frac{I_2(\ell)}{\ell} & & & \text{Symmetric} & & \\
\frac{2I_3(\ell)}{\ell^2} & 0 & 0 & \frac{I_3(\ell)}{\ell} & & & & \\
-\frac{6I_3(\ell)}{\ell^3} & 0 & 0 & -\frac{2I_3(\ell)}{\ell^2} & \frac{6I_3(\ell)}{\ell^3} & & & \\
0 & -\frac{6I_2(\ell)}{\ell^3} & \frac{2I_2(\ell)}{\ell^2} & 0 & 0 & \frac{6I_2(\ell)}{\ell^3} & & \\
0 & -\frac{4I_2(\ell)}{\ell^2} & \frac{I_2(\ell)}{\ell} & 0 & 0 & \frac{4I_2(\ell)}{\ell^2} & \frac{3I_2(\ell)}{\ell} & \\
\frac{4I_3(\ell)}{\ell^2} & 0 & 0 & \frac{I_3(\ell)}{\ell} & -\frac{4I_3(\ell)}{\ell^2} & 0 & 0 & \frac{3I_3(\ell)}{\ell}
\end{bmatrix}
$$

$$
\underset{\sim}{M} = \frac{\rho A(0)}{840} \begin{bmatrix}
240\ell & & & & & & & \\
0 & 240\ell & & & & & & \\
0 & -30\ell^2 & 5\ell^3 & & & \text{Symmetric} & & \\
30\ell^2 & 0 & 0 & 5\ell^3 & & & & \\
54\ell & 0 & 0 & 12\ell^2 & 72\ell & & & \\
0 & 54\ell & -12\ell^2 & 0 & 0 & 72\ell & & \\
0 & 14\ell^2 & -3\ell^3 & 0 & 0 & 14\ell^2 & 3\ell^3 & \\
-14\ell^2 & 0 & 0 & -3\ell^3 & -14\ell^2 & 0 & 0 & 3\ell^3
\end{bmatrix} + \frac{\rho A(\ell)}{840} \begin{bmatrix}
72\ell & & & & & & & \\
0 & 72\ell & & & & & & \\
0 & -14\ell^2 & 3\ell^3 & & & \text{Symmetric} & & \\
14\ell^2 & 0 & 0 & 3\ell^3 & & & & \\
54\ell & 0 & 0 & 14\ell^2 & 240\ell & & & \\
0 & 54\ell & -14\ell^2 & 0 & 0 & 240\ell & & \\
0 & 14\ell^2 & -3\ell^3 & 0 & 0 & 30\ell^2 & 5\ell^3 & \\
-12\ell^2 & 0 & 0 & -3\ell^3 & -30\ell^2 & 0 & 0 & 5\ell^3
\end{bmatrix}
$$

FIGURE I-1.--Mass ($\underset{\sim}{M}$) and Stiffness ($\underset{\sim}{K}$) Arrays

for viscoelastic materials can be replaced by the relaxation modulus utilizing the correspondance principle. Second, if

$$I(0) = I(L)$$

$$A(0) = A(L)$$

then the mass and stiffness arrays are identical to those found in Przemieniecki.

APPENDIX II

COMPUTER PROGRAM

The following appendix briefly describes the development of the ten computer programs used for this study. The details of each routine are not discussed, however, data information flow from program to program (see Figure II-1) and a short description of the functions of each program are presented here.

XRPLOT creates a computer generated overlay used for extracting data from a leg x-ray. The overlay specifies data points, on the x-ray, which are to be used in the XRDAT program. Input to the program is tibia length.

XRDAT is a data file, created by the operator, containing data points specified by XRPLOT. This program is simply a data 'holding' program for information used in generating the finite element model. The routine stores information in a data buffer which is accessible to FINEL as input data. The advantage of this method is that the data base is independent of all other programs, and several XRDAT files, each representing different x-rays, can be created and used at the operator's discretion. Upon reception of XRDAT data, FINEL creates all the nodal points for the finite element model. These data are output to a buffer from which several programs take information (see Figure II-1).

FLESHPLOT and BIGPLOT are plot routines used as a check for the finite element model, as any erroneous data points will show up clearly on these plots. FLESHPLOT produces a cross section view of the leg at

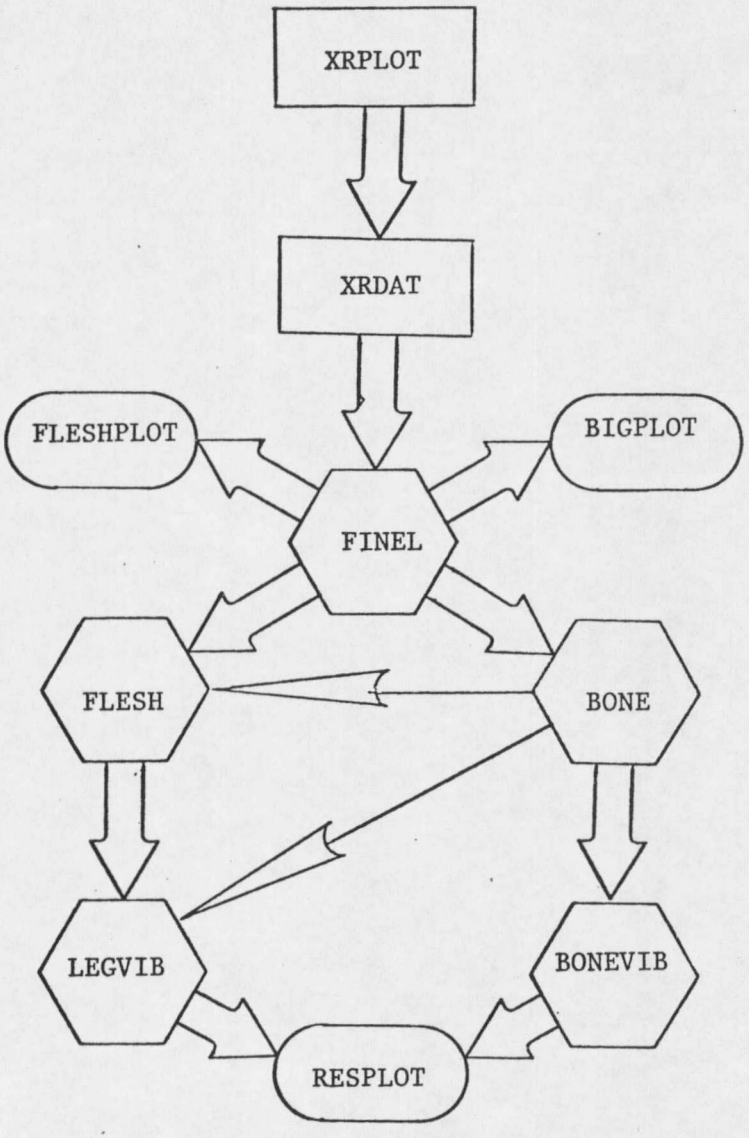

FIGURE II-1.--Flow Diagram

any of the eleven leg cross sections. BIGPLOT generates, at any rotated view, a three-dimensional bone structure plot of the entire lower leg. Examples of FLESHPLOT and BIGPLOT are Figures 1 and 4 respectively. These programs have no direct bearing on the solution, however, they are an effective debugging aid.

BONES and FLESH create the bone and flesh, mass and stiffness, arrays for the finite element model from FINEL data. $\underset{\sim}{\gamma}$ is also developed within these routines, and applied to the arrays. Again, output is stored in a buffer for later use. LEGVIB and BONEVIB are then used to generate the dynamic response of the lower leg model. BONEVIB utilizes only bone data and generates the response of just the tibia, whereas LEGVIB adds the fibula and flesh to the system. Thus, BONEVIB can be used for correlating excised tibia experimental data with theoretical data, and LEGVIB can be used to determine the effects of adding flesh to the system. Both programs also have the capability of applying viscoelastic support end conditions to the bone model. RESPLOT then produces a plot of frequency vs. amplitude of acceleration for the system from data generated by either BONEVIB or LEGVIB.

REFERENCES

1. Jurist, J. and K. Kianian, "Three Models of the Vibrating Ulna, J. Biomechanics 6, pp. 331-342, 1973.
2. Doherty, W. P., E. G. Bovill, and E. L. Wilson, "Evaluation of the Use of Resonant Frequencies to Characterize Physical Properties of Human Long Bones," J. Biomechanics 7, pp. 559-562, 1974.
3. Spiegl, P. V., and J. M. Jurist, "Prediction of Ulnar Resonant Frequency," J. Biomechanics 8, pp. 213-217, 1975.
4. Orne, D., "The In Vivo, Driving-Point Impedance of the Human Ulna--A Viscoelastic Beam Model," J. Biomechanics 7, pp. 249-257, 1974.
5. Orne, D. and J. Mandke, "The Influence of Musculature on the Mechanical Impedance of the Human Ulna, an In Vivo Simulated Study," J. Biomechanics 8, pp. 143-149, 1975.
6. Garner, E. G., "Determination of Macroscopic Biological Material Properties by Dynamic, 'In-Vivo' Testing," thesis for the degree of Doctor of Philosophy, Mechanical Engineering Department, Montana State University, August 1973.
7. Orne, D. and D. R. Young, "The Effects of Variable Mass and Geometry, Pretwist, Shear Deformation and Rotatory Inertia on the Resonant Frequencies of Intact Long Bones: A Finite Element Model Analysis," J. Biomechanics 9, pp. 763-770, 1976.
8. Przemieniecki, J. S., Theory of Matrix Structural Analysis, McGraw-Hill, 1968.

9. Flugge, W., Viscoelasticity, Second Edition, Springer-Verlag, 1975.

10. Meirovitch, L., Analytical Methods in Vibrations, Macmillan, 1967.

11. Bargren, J. H., C. A. L. Bassett, and A. Gjelsvik, "Mechanical Properties of Hydrated Cortical Bone," J. Biomechanics 7, pp. 239-245, 1974.

12. Reilly, D. T., A. L. Burstein, and V. H. Frankel, "The Elastic Modulus for Bone," J. Biomechanics 7, pp. 271-275, 1974.

13. Hayes, W. C., L. W. Swenson, Jr., and D. J. Schurman, "Axisymmetric Finite Element Analysis of the Laterial Tibial Plateau," J. Biomechanics 11, pp. 21-33, 1978.

14. Harrigan, M. D., "Development of Equipment and Techniques for Experimental Determination of Dynamic Response of the Human Forearm," thesis for Master of Science degree, Mechanical Engineering, Montana State University, August 1974.

Johnson, Douglas Wayne
Dynamic response model of the human leg

DATE	ISSUED TO
[illegible]	[illegible] PATTI MCGUIRE [illegible]